Probing nodeless superconductivity in La M Si (M=Ni, Pt) using muon-spin rotation and relaxation

Sajilesh K. P., D. Singh, A. D. Hillier, and R. P. Singh

Published version information

Citation: KP Sajilesh et al. "Probing nodeless superconductivity in La M Si (M=Ni, Pt) using muon-spin rotation and relaxation." Phys Rev B 102, no. 9 (2020): 094515.

DOI: 10.1103/PhysRevB.102.094515

Probing nodeless superconductivity in La*M*Si (*M*=Ni, Pt) using muon-spin rotation and relaxation

Sajilesh K. P.,[1] D. Singh,[2] A. D. Hillier,[2] and R. P. Singh[1,*]

[1]*Department of Physics, Indian Institute of Science Education and Research Bhopal, Bhopal 462066, India*

[2]*ISIS Facility, STFC Rutherford Appleton Laboratory, Harwell Science and Innovation Campus, Oxfordshire OX11 0QX, United Kingdom*

(Received 11 February 2020; revised 4 September 2020; accepted 8 September 2020; published 22 September 2020)

Systems with strong spin-orbit coupling have been a topic of fundamental interest in condensed matter physics due to the exotic topological phases and the unconventional phenomenon they exhibit. In this particular study, we have investigated the superconductivity in the transition-metal ternary noncentrosymmetric compounds La*M*Si (*M*=Ni, Pt) with different spin-orbit coupling strength, using muon-spin rotation and relaxation measurements. Transverse-field measurements made in the vortex state indicate that the superconductivity in both materials is fully gapped, with a conventional *s*-wave pairing symmetry and BCS-like magnitudes for the zero-temperature gap energies. Zero-field measurements suggest a time-reversal symmetry preserved superconductivity in both the systems, though a small increase in muon depolarization is observed upon decreasing temperature. However, this has been attributed to quasistatic electronic fluctuations.

DOI: 10.1103/PhysRevB.102.094515

I. INTRODUCTION

Noncentrosymmetric (NCS) materials are unique candidates to explore exotic features such as unconventional superconductivity and topologically protected surface states [1–3]. These remarkable materials possess an antisymmetric spin-orbit coupling, causing the formation of two spin-dependent Fermi surfaces. This, in general, can lead to the Cooper pair forming with a mixed singlet-triplet character [4–9]. Such a scenario can lead to zero's/multiple gaps in the energy spectrum, time-reversal symmetry breaking (TRSB), and topologically protected nontrivial surface states [10–14]. A breakthrough discovery occurred when the line nodes in the heavy-fermion compound $CePt_3Si$ were found, followed by triplet pairing and nodes in weakly correlated $Li_2(Pd,Pt)_3B$ [10,12]. This has shown the immense potential of NCS materials to host unconventional superconductivity. $Li_2(Pd,Pt)_3B$ is one of the most acclaimed compounds where the antisymmetric spin-orbit coupling (ASOC) effects have been directly observed. Li_2Pt_3B has shown the presence of triplet and line node, while Li_2Pd_3B with the same structure has shown conventional *s*-wave behavior [12,15,16]. The unusual properties of Li_2Pt_3B are attributed to the increase in ASOC which is proportional to Z^4. Besides this, line nodes in the superconducting gap are discovered for $CeIrSi_3$ [17] and $K_2Cr_3As_3$ [18,19], while multiple nodeless gaps were shown by $LaNiC_2$ [20] and $(La,Y)_2C_3$ [21]. In addition, these materials are expected to possess topologically protected flat zero-energy bands of surface states, which can be termed as a long-sought Majorana fermion [22–26].

A few transition-metal superconductors including La_7Ir_3 [27] and Re_6X (*X*=Zr, Hf, Ti) [28–30] with strong ASOC have shown a spontaneous field upon entering the superconducting state and hence TRSB. Meanwhile, $LaNiC_2$ with noncentrosymmetric structure and low ASOC has also shown TRSB [31,32]. Moreover, in a similar case, $LaNiGa_2$, with centrosymmetric structure and low ASOC, has shown

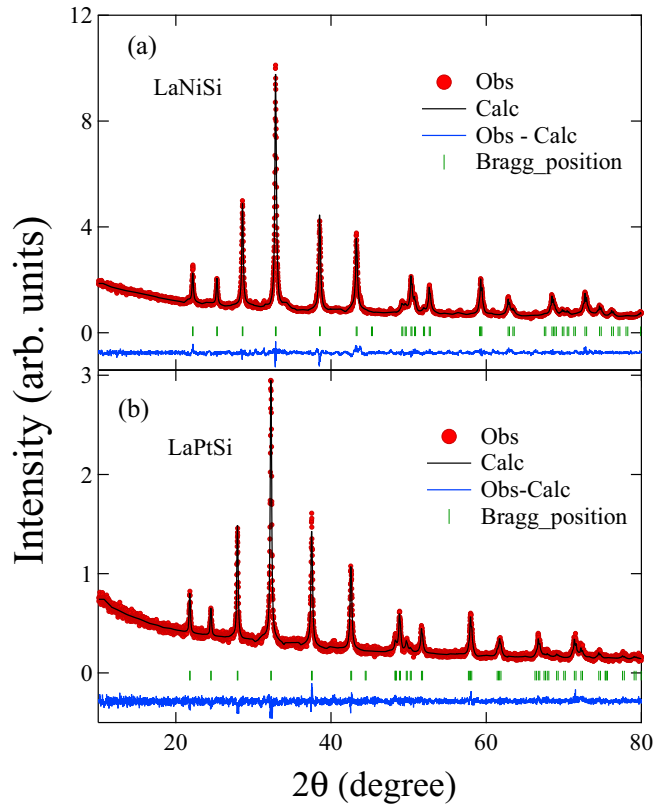

FIG. 1. X-ray diffraction pattern collected at ambient conditions for (a) LaNiSi and (b) LaPtSi refined with noncentrosymmetric α-$ThSi_2$-type structure.

*rpsingh@iiserb.ac.in

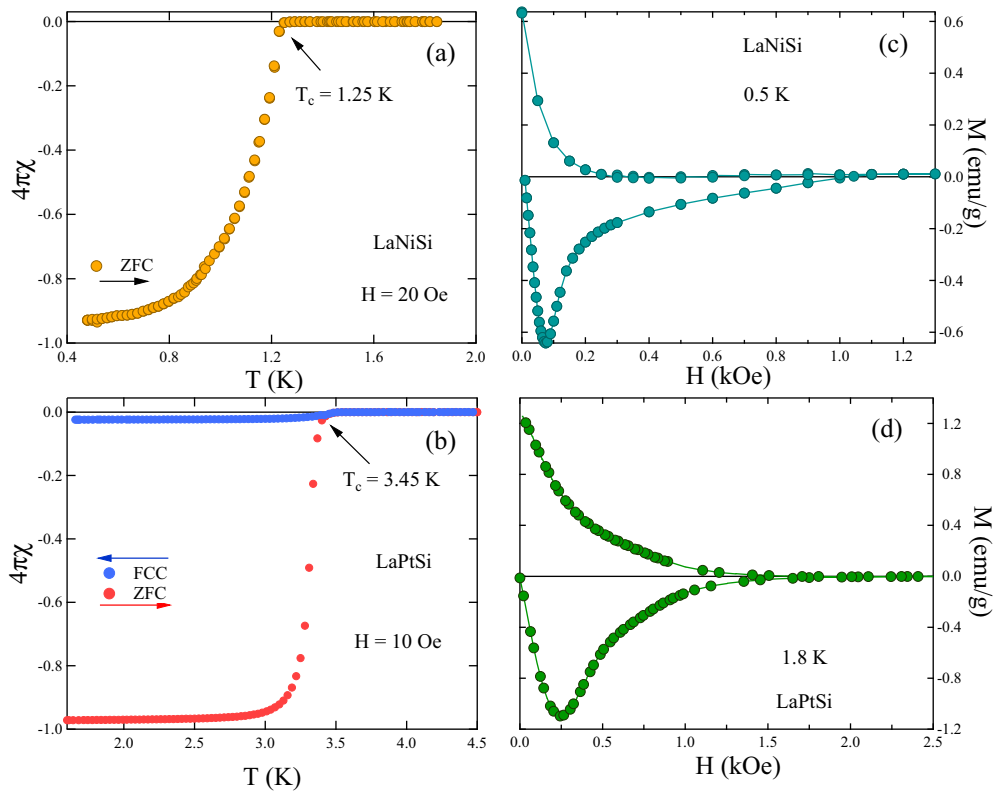

FIG. 2. (a) and (b) Magnetization data collected at ZFC-FC mode showing the superconducting transition at 1.25 and 3.45 K, respectively, for LaNiSi and LaPtSi. (c) and (d) *M*-*H* curve taken at the superconducting regime showing a type-II behavior by both compounds.

spontaneous field in the superconducting state, questioning the role played by ASOC [33]. Also, many materials with considerably large ASOC have failed to show any nontrivial superconductivity [34–38].

The recent discovery of TRSB in pure Re metal has further increased the curiosity in this field, raising more open questions regarding the emergence of TRSB [39]. The strength of the TRSB signal in Re-based binary systems (Re_6X) has remained unaltered, irrespective of the transition element used. Though the microscopic origin of TRSB in these compounds is still unknown, the local electronic structure of Re might be playing a crucial role. Hence it is important to search for more NCS materials with different ASOC strength to elucidate the effects of ASOC on the superconducting ground state.

Since significant spin-orbit coupling is a proposed necessary criterion to exhibit exotic properties, we turned our focus onto La-based NCS systems, LaNiSi and LaPtSi. Both of them crystallize in LaPtSi-type structure, while the spin-orbit coupling has different values as Pt is a heavier element compared to Ni [40–42]. Pt being a *d*-block element with the third-largest atomic number is expected to induce a stronger ASOC. A recent theoretical study on a similar structure compound, Th*T*Si (*T*=Co, Ir, Ni, and Pt), has shown that ASOC has caused splitting of the Fermi surface into two nondegenerate subbands with different helicity [43]. It was also noticed that this effect is stronger for the case of Ir and Pt, which have heavier mass. Hence a microscopic investigation on La*M*Si can explicate the effect of similar Fermi surface splitting on the superconducting ground state. Furthermore, the contribution to the electronic density of states at Fermi energy, including the spin-orbit coupling, is dominated by the Pt-*d* band [44,45]. Hence, a comparative study with the lighter Ni atom in place of Pt gives an opportunity to unravel the effects of ASOC and density of states on the superconducting ground state. In addition to this, recent findings of rich topological features such as nontrivial nodal rings of Weyl type and the possibility to show topological Hall effect makes La*M*Si a worthy candidate for study [44].

Here, we have used muon-spin rotation/relaxation measurement (μSR) to investigate the superconducting ground state. Zero-field (ZF) μSR is exceptionally sensitive to intrinsic local magnetization arising at the superconducting phase transition in the case of an unconventional pairing mechanism. In addition, the transverse field (TF) μSR is an excellent tool to probe the superconducting gap structure. It can accurately probe the penetration depth in superconductors, and measuring the temperature dependence provides details of the gap structure. This technique has already been used in unraveling the unconventional nature of many superconductors. It has been widely used in materials including heavy-fermion superconductors [46,47], Fe-based superconductors [48], and other alloy-based superconductors [27–30,39] giving path-breaking results.

II. EXPERIMENTAL METHODS

Polycrystalline samples of LaNiSi and LaPtSi were prepared by arc melting stoichiometric amounts of the constituent elements on a water-cooled copper hearth under argon gas atmosphere. The samples were flipped and remelted several

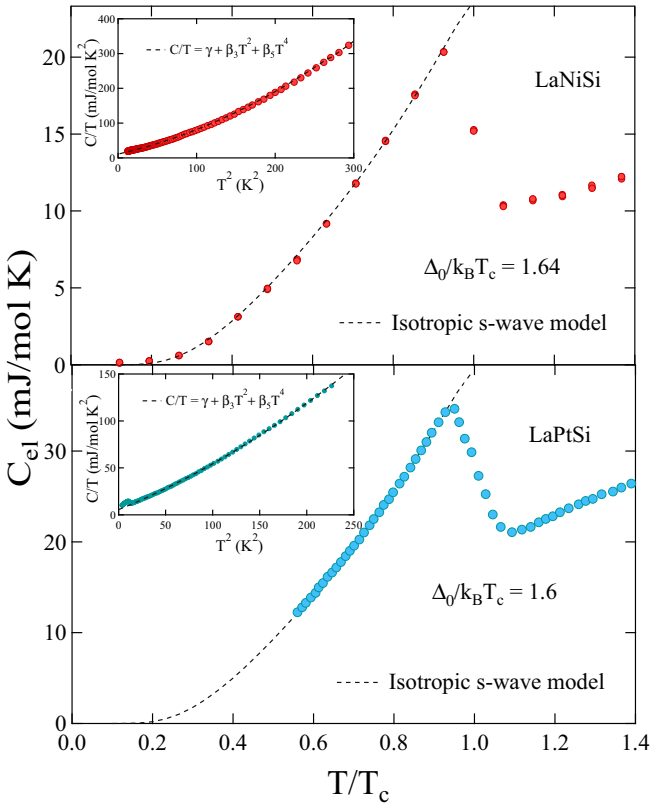

FIG. 3. Temperature-dependent electronic specific heat data for both LaNiSi and LaPtSi taken at 0 T. The superconducting region can be well traced by the isotropic BCS s-wave model, giving the normalized specific heat jump as 1.64 and 1.6, respectively, for LaNiSi and LaPtSi. The insets show the total specific heat data plotted as C/T vs T^2.

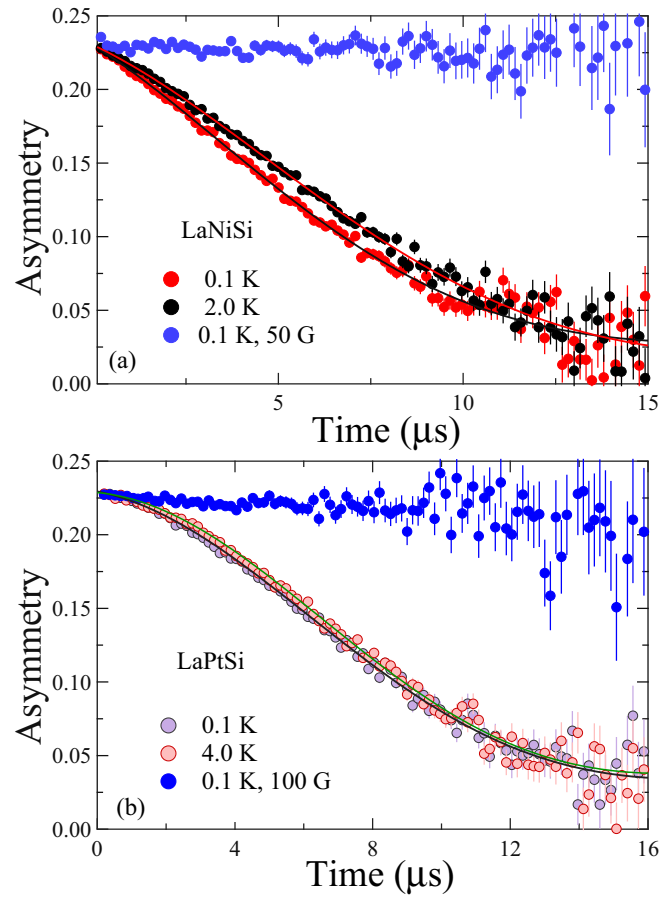

FIG. 4. Time evolution of the spin polarization of muons implanted under zero-field conditions in (a) LaNiSi and (b) LaPtSi at temperatures above and below T_c. The solid lines are the results of fitting the data to Eq. (2). Blue markers show the muon depolarization at a small longitudinal applied field.

times to ensure the homogeneity of the ingot. There was no measurable weight loss during the melting. All samples were wrapped in Ta foil, sealed in quartz ampoules under vacuum, and annealed at 800 °C for 1 week to remove any thermal strain. The sample characterization was done using x-ray powder diffraction on a PANalytical diffractometer using Cu $K\alpha$ radiation ($\lambda = 1.540\,56$ Å). Magnetic susceptibility measurements were performed on a magnetic property measurement system superconducting quantum interference device magnetometer (Quantum Design). Heat capacity measurements were performed using a Quantum Design physical property measurement system. The muon-spin relaxation/rotation (μSR) measurements were carried out using the MUSR spectrometer at the ISIS Neutron and Muon Facility in STFC Rutherford Appleton Laboratory, United Kingdom. The powdered samples of LaMSi (M=Ni, Pt) were mounted on a high-purity-silver plate using diluted GE varnish. For LaNiSi, the measurements were performed in the temperature range 0.1–2.0 K, whereas, for LaPtSi, the measurements were made between 0.1 and 4.0 K. The μSR measurements were performed under longitudinal and transverse-field geometry. During measurement, spin-polarized muons were implanted into the sample. The implanted muons precess according to the local magnetic field distribution and emit positrons during decay after a lifetime of 2.2 μs. The distribution of positrons gives vital information regarding the nature of internal field distribution. In zero-field configuration, the stray fields at the sample position due to neighboring instruments and the Earth's magnetic field are canceled to within ~1.0 μT using three sets of orthogonal coils. In the transverse configuration, a field was applied perpendicular to the direction of the muon spin (which is opposite to muons linear momentum), and the detectors were grouped into two orthogonal pairs. A full description of the μSR technique may be found in Ref. [49].

III. RESULTS AND DISCUSSION

Powder x-ray diffraction data were collected for both the samples. Rietveld refinement of the data confirmed that both samples had crystallized into the tetragonal, noncentrosymmetric structure with space group $I4_1md$ (109) (Fig. 1). The lattice parameters of LaNiSi [$a = b = 4.1800(3)$ Å, $c = 14.0780(8)$ Å] and LaPtSi [$a = b = 4.2466(8)$ Å, $c = 14.5213(4)$ Å] obtained in this work are in good agreement with data reported previously in Refs. [41,42].

The samples were characterized using the dc susceptibility measurements in zero-field-cooling and field-cooling modes under an applied magnetic field. The appearance of a strong

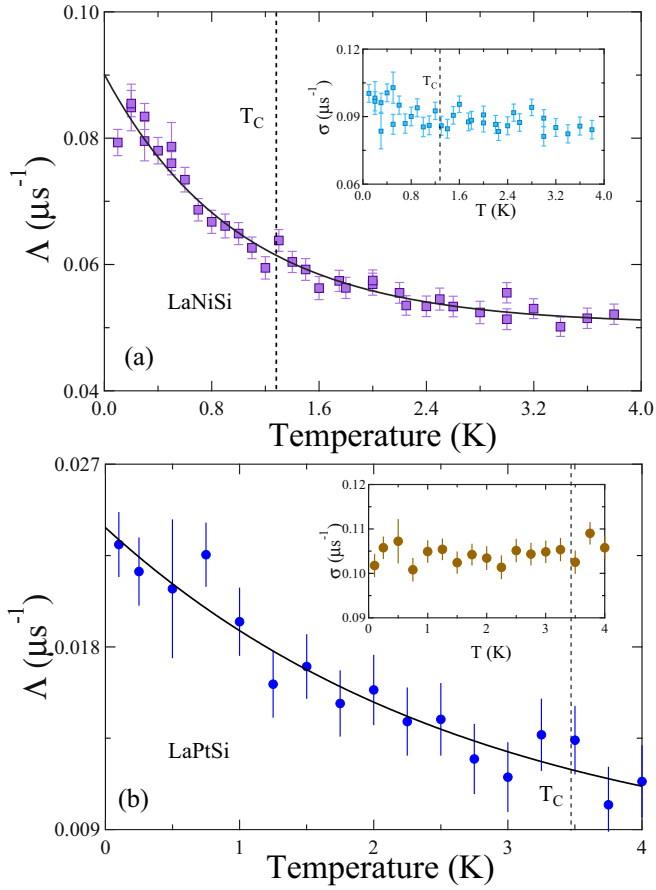

FIG. 5. Temperature dependence of the electronic relaxation rate in (a) LaNiSi and (b) LaPtSi, collected in ZF. The solid lines are guides to the eye, indicating the exponential decay of Λ in ZF as T is increased. The insets show the constant behavior of nuclear relaxation rate σ across the transition temperature.

diamagnetic signal at $T_c = 1.25 \pm 0.02$ K in LaNiSi and $T_c = 3.45 \pm 0.04$ K in LaPtSi confirms the bulk superconducting nature [Figs. 2(a) and 2(b)]. The Meissner volume fraction $4\pi\chi$ for both samples is less than 100% due to uncorrected geometrical shape factor. Magnetization measurements exhibit no other magnetic anomalies that may be due to impurities in the sample.

Figures 2(c) and 2(d) show the magnetization data collected below the superconducting transition temperature for both the samples. Magnetization data shows a linear behavior at low field, after which the sample enters a vortex state. This clearly depicts the type-II nature of the sample.

Further investigation on the superconducting nature was done by temperature-dependent specific heat analysis. A superconducting anomaly for both the samples was observed at $T_c = 1.11$ and 3.4 K (Fig. 3). The normal-state specific heat for the samples above T_c can be described by $C = \gamma T + \beta_3 T^3 + \beta_5 T^5$. This gave the fitting parameters as $\gamma_n = 9.12 \pm 0.07$ mJ/mol K^2, $\beta_3 = 0.487 \pm 0.001$ mJ/mol K^4, and $\beta_5 = (1.98 \pm 0.01) \times 10^{-4}$ mJ/mol K^6 for LaNiSi while for LaPtSi it is $\gamma_n = 4.72 \pm 0.22$ mJ/mol K^2, $\beta_3 = 0.423 \pm 0.004$ mJ/mol K^4, and $\beta_5 = (7.34 \pm 0.01) \times 10^{-4}$mJ/mol K^6. Several parameters characterizing the materials can be deduced using these values and are shown in Table I. The electronic specific heat in the superconducting region is well explained by an isotropic s-wave model, giving the normalized superconducting gap, $\Delta_0/k_B T_c = 1.64 \pm 0.04$ and 1.61 ± 0.05, respectively, for LaNiSi and LaPtSi.

TABLE I. Normal and superconducting properties of La(Ni,Pt)Si.

Parameter	Unit	LaNiSi	LaPtSi
T_c	K	1.25 ± 0.02	3.45 ± 0.04
θ_D	K	230 ± 3	239 ± 2
$\lambda_{e\text{-}ph}$		0.48 ± 0.02	0.61 ± 0.02
$D_c(E_f)$	$\frac{\text{states}}{\text{eV f.u.}}$	3.87 ± 0.12	1.99 ± 0.06
$\Delta(0)/k_B T_c$		1.63 ± 0.04	1.74 ± 0.05
m^*/m_e		1.48 ± 0.06	1.61 ± 0.13
n	10^{26} m^{-3}	3.37 ± 0.36	8.85 ± 0.86
λ_L	nm	352 ± 19	226 ± 11
T_F	K	1380 ± 90	2430 ± 157

A systematic ZF-μSR measurement can be used to detect any spontaneous magnetization below the superconducting transition. We performed the ZF-μSR relaxation experiments on both LaMSi (M=Ni, Pt) samples and Fig. 4 shows the ZF-μSR spectra for both samples at selected temperatures above and below T_c. Below T_c, there is a clear change in the relaxation behavior in both compounds. The relaxation became faster with the decreasing temperature down to the lowest temperature, although the difference is much subtler in LaPtSi. Notably, there is no sign of an oscillatory component which would otherwise indicate coherent field associated with magnetic ordering. In the absence of atomic moments, the relaxation is due to the presence of static, randomly oriented local fields associated with the nuclear moments. The ZF-μSR data can be well described by a damped Gaussian Kubo-Toyabe (KT) function:

$$G(t) = A_1 \exp(-\Lambda t) G_{\mathrm{KT}}(t) + A_{\mathrm{BG}}, \tag{1}$$

where A_1 is the sample asymmetry, Λ is the additional relaxation rate, and A_{BG} is the background asymmetry. The $G_{\mathrm{KT}}(t)$ function is the Gaussian Kubo-Toyabe function given by [50]

$$G_{\mathrm{KT}}(t) = \frac{1}{3} + \frac{2}{3}\left(1 - \sigma_{\mathrm{ZF}}^2 t^2\right) \exp\left(\frac{-\sigma_{\mathrm{ZF}}^2 t^2}{2}\right), \tag{2}$$

where $\sigma_{\mathrm{ZF}}/\gamma_\mu$ is the local-field distribution width, $\gamma_\mu = 135.53$ MHz/T being the muon gyromagnetic ratio. The parameters A_1 and A_{BG} extracted by fitting the ZF-μSR spectra using Eq. (1) are found to be temperature independent for both the samples. The temperature dependence of the fit parameters σ_{ZF} and Λ for LaNiSi and LaPtSi are displayed in Figs. 5(a) and 5(b). Again, the nuclear term σ_{ZF} is found to be approximately temperature independent in both compounds (see Fig. 5 insets). In contrast, the additional relaxation rate, Λ, can be seen to increase gradually with decreasing temperature (shown in Fig. 5). There is no distinct anomaly at T_c. Therefore, the observed behavior, we believe, could not be associated with the superconducting nature of the samples. The exponential character of $\Lambda(T)$ in both materials reveals the existence of fast electronic fluctuations measurable within the μSR time window. A decrease in fluctuation

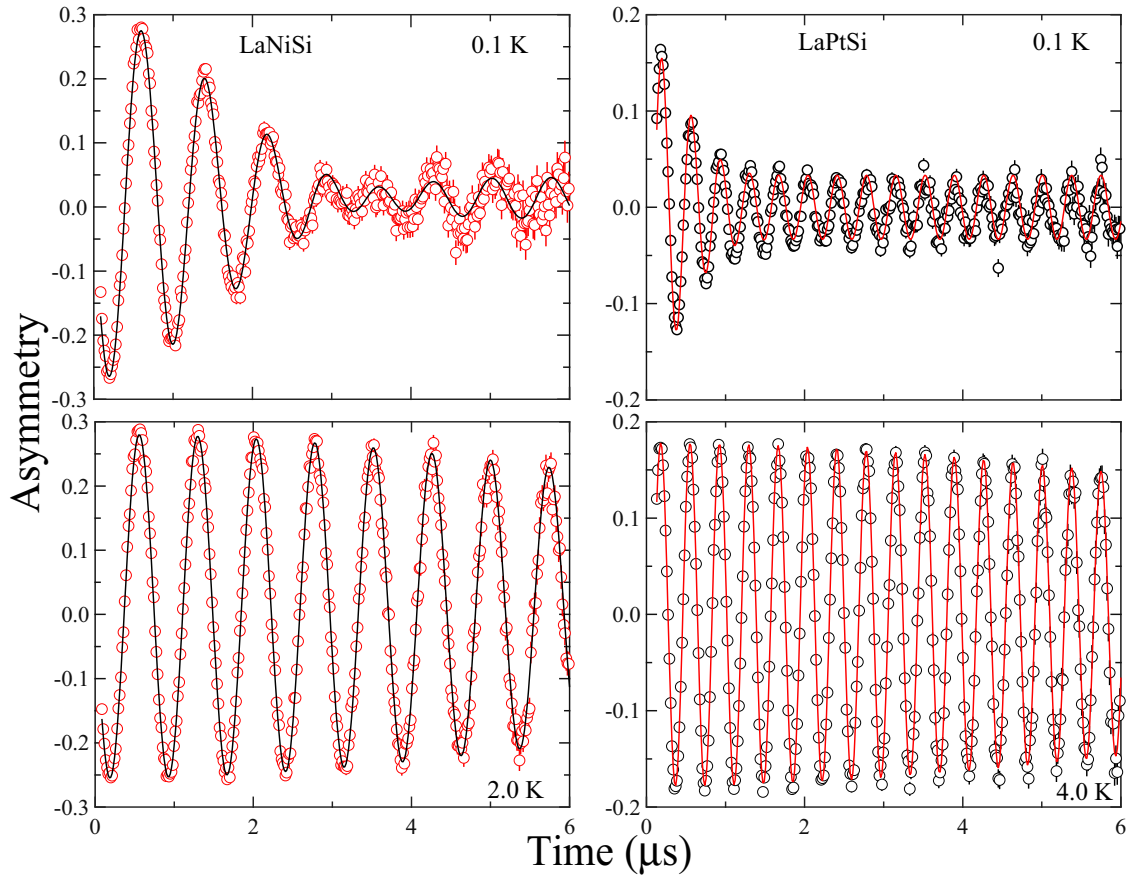

FIG. 6. Transverse-field muon time spectra collected in a magnetic field $H = 100$ Oe at 0.1 and 2.0 K for the LaNiSi (top left and bottom left) and in a magnetic field $H = 200$ Oe at 0.1 and 4.0 K for the LaPtSi (top right and bottom right).

frequency of electronic moments as temperature decreases may cause Λ to increase. Similar behavior is observed in a number of superconductors [51–53]. However, the exact nature and source of this behavior is still unknown and therefore requires further investigation. The nature of ZF relaxation can be further explored by the application of the longitudinal field. In both materials, a small longitudinal field is sufficient to decouple the static fields completely, with the overall depolarization being minimized. This implies that the fluctuations responsible for this relaxation channel are in fact static or quasistatic with respect to the muon lifetime, and the magnitude of the fluctuations is $\leqslant 100$ Oe.

TF-μSR is an excellent tool to explore the gap structure of superconducting materials. We have performed a TF-μSR experiment down to a temperature of 0.1 K in order to probe the flux line lattice and therefore determine the symmetry of the superconducting gap. Figure 6 shows the μSR precession signals below and above T_c for both the LaNiSi and LaPtSi compounds. The data were collected in an applied field of $H = 100$ Oe for LaNiSi and $H = 200$ Oe for LaPtSi. The field was applied above T_c before cooling down to 0.1 K in order to ensure that the samples are in the mixed state. Figure 6 (bottom) show the spectra above T_c for both the samples where the spectra oscillate with a frequency that corresponds to the Larmor precession, damped with a weak Gaussian relaxation due to the nuclear dipole field. Below T_c, the signal decays with time due to the inhomogeneous field distribution from the flux line lattice [shown in Fig. 6 (top)]. To quantitatively analyze the experimental data, the following oscillatory decaying Gaussian function was employed:

$$G_{\rm TF}(t) = A_0 \exp\left(\frac{-\sigma^2 t^2}{2}\right)\cos(\omega_1 t + \phi) + A_1 \cos(\omega_2 t + \phi). \quad (3)$$

Here A_0 and A_1 are the initial asymmetries of the sample and background signals, ω_1 and ω_2 are the precession frequencies of muons from the sample and silver holder, respectively, ϕ is the phase offset of the initial muon-spin polarization with respect to the positron detector, and σ is the depolarization rate. The inset of Fig. 7 shows the temperature dependence of the internal magnetic field, calculated from the muon precession frequency. The flux expulsion at T_c is evident from the reduction of the average field $\langle B \rangle$ inside the superconductor, and the corresponding background field $B_{\rm bg}$ is approximately constant over the temperature range. The muon depolarization rate σ extracted from Eq. (3) is comprised of the following terms: $\sigma^2 = \sigma_{\rm sc}^2 + \sigma_{\rm N}^2$, where $\sigma_{\rm sc}$ is the depolarization arising due to the field variation across the flux line lattice and $\sigma_{\rm N}$ is the contribution due to nuclear dipolar moments. The superconducting contribution to depolarization $\sigma_{\rm sc}$ is calculated by subtracting $\sigma_{\rm N}$ from total σ.

The temperature dependence of σ is seen nearly constant below $\simeq T_c/3$ for both compounds. This possibly suggests

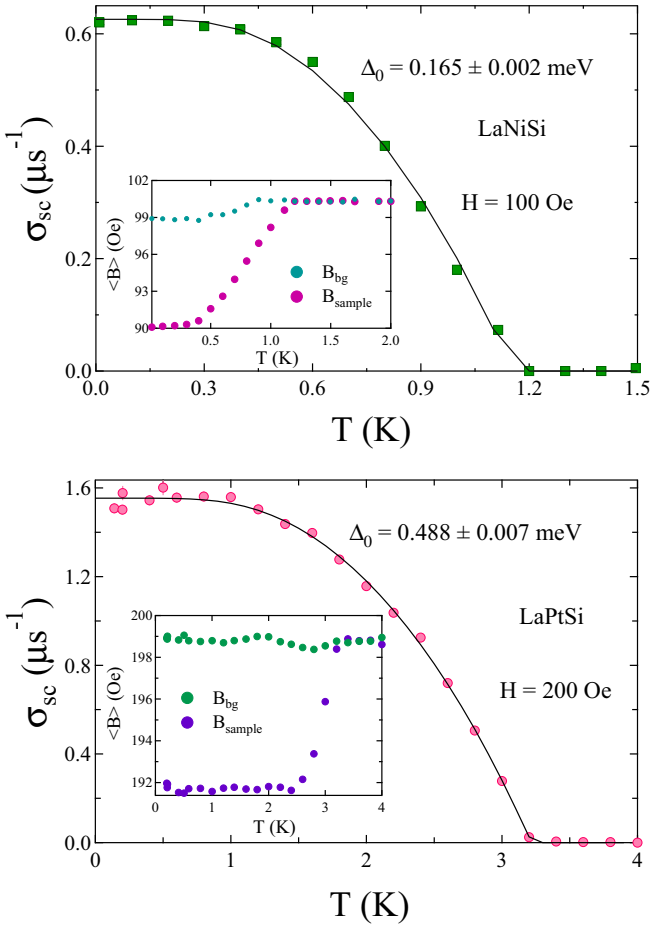

FIG. 7. Temperature dependence of σ_{sc} measured at an applied field. The solid line is the dirty limit isotropic *s*-wave fit for the data. The inset shows the internal field variation for the samples.

the absence of nodes in the superconducting energy gap at the Fermi surface. The solid line in Fig. 7 represents the temperature dependence of the muon depolarization rate $\sigma(T)$ within the local London approximation for an *s*-wave BCS superconductor in the dirty limit:

$$\frac{\sigma_{\mathrm{FLL}}^{-2}(T)}{\sigma_{\mathrm{FLL}}^{-2}(0)} = \frac{\Delta(T)}{\Delta(0)} \tanh\left[\frac{\Delta(T)}{2k_BT}\right], \tag{4}$$

where $\Delta(T)/\Delta(0) = \tanh\{1.82[1.018(T_c/T - 1)]^{0.51}\}$ is the BCS approximation for the temperature dependence of the energy gap and $\Delta(0)$ is the gap magnitude at zero temperature. Whereas in the clean limit, the expression is given by

$$\frac{\sigma_{\mathrm{FLL}}^{-2}(T)}{\sigma_{\mathrm{FLL}}^{-2}(0)} = 1 + 2\int_{\Delta(T)}^{\infty} \left(\frac{\delta f}{\delta E}\right) \frac{EdE}{\sqrt{E^2 - \Delta^2(T)}}. \tag{5}$$

Here, $f = [1 + \exp(E/k_BT)]^{-1}$ is the Fermi function and $\Delta(T) = \Delta_0\delta(T/T_c)$. $\delta(T/T_c) = \tanh\{1.82[1.018(T_c/T - 1)]^{0.51}\}$ is the temperature dependence of the energy gap. We have obtained a good fit for the data using the dirty limit model giving values of the superconducting gap as $\Delta_0 = 0.197 \pm 0.003$ meV and 0.488 ± 0.007 meV for LaNiSi and LaPtSi, respectively. This gives the normalized value of the superconducting gap $\frac{\Delta(0)}{k_BT_c}$ as 1.63 and 1.74, respectively, for

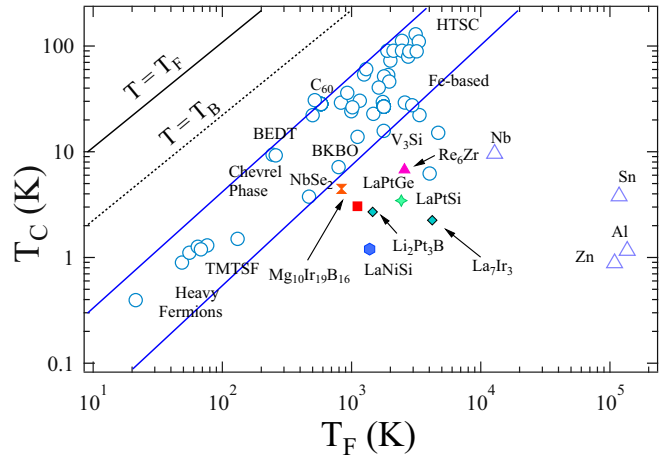

FIG. 8. Uemura plot showing T_c vs the effective Fermi temperature T_F. The blue band represents different families of superconductors with unconventional properties. The positions of LaNiSi and LaPtSi indicate a conventional nature of these materials.

LaNiSi and LaPtSi, showing a moderately coupled nature of samples consistent with previous reports [41,42].

In a superconductor with ideal Ginzburg-Landau vortex lattice, Brandt has explained the relation between the magnetic penetration length λ and the muon depolarization rate σ_{sc} [54,55]. According to this, for a superconductor with$h = H/H_{c2} \leqslant 0.25$,

$$\sigma_{\mathrm{FLL}}[\mu s^{-1}] = 4.854 \times 10^4(1 - h)[1 + 1.21(1 - \sqrt{h})^3]\lambda^{-2}[\mathrm{nm}^{-2}]. \tag{6}$$

Substituting the value of σ_{sc} gives $\lambda = 352 \pm 19$ nm and 226 ± 11 nm for LaNiSi and LaPtSi, respectively. Using this, we estimated the superconducting carrier density n_s, by $n_s(0) = \frac{m^*}{\mu_0 e^2 \lambda^2}$, where $m^* = (1 + \lambda_{e\text{-}ph})m_e$. We have used θ_D obtained from specific heat measurement to calculate $\lambda_{e\text{-}ph} = 0.48 \pm 0.02$ for LaNiSi and $\lambda_{e\text{-}ph} = 0.61 \pm 0.02$ for LaPtSi. These values are in excellent agreement with theoretical predictions [44]. Substituting this has given the superconducting carrier density as $(3.37 \pm 0.36) \times 10^{26}/\mathrm{m}^3$ and $(8.85 \pm 0.86) \times 10^{26}/\mathrm{m}^3$ for LaNiSi and LaPtSi, respectively. This can be used to calculate the Fermi temperature for the materials using the relation

$$k_BT_F = \frac{\hbar^2}{2}(3\pi^2)^{2/3}\frac{n_s^{2/3}}{m^*}. \tag{7}$$

The obtained values for T_F are 1380 ± 98 K and 2430 ± 157 K, respectively. The values are close to those reported elsewhere for transition-metal alloys [56]. This can be further used to classify the superconductors as done by Uemura *et al.* [57–60]. According to the Uemura classification scheme, high-temperature superconductors, heavy-fermionic superconductors, Fe-based superconductors, and other exotic superconductors fall in the range $0.01 \leqslant \frac{T_c}{T_F} \leqslant 0.1$. For conventional BCS superconductors, $\frac{T_c}{T_F} \leqslant 0.001$. The value of $\frac{T_c}{T_F} = 0.0008$ and 0.0014 for LaNiSi and LaPtSi places both the compounds away from the unconventional band of

superconductors, as shown in Fig. 8, but close to other superconductors that may be considered as exotic, such as the nickelborocarbides [60]. Calculated superconducting parameters are tabulated in Table I.

IV. CONCLUSION

We have probed the superconducting properties of ternary equiatomic silicides LaM (M=Ni, Pt)Si by magnetization, specific heat, and muon-spin rotation and relaxation measurements. The specific heat measurements have indicated an s-wave nature for both the samples. A systematic TF-μSR study at an applied field reveals the T_c for the samples as 1.2 and 3.45 K, respectively, for LaNiSi and LaPtSi with both showing a type-II nature. A temperature-independent nature of muon depolarization rate at low temperatures ruled out the presence of any anisotropic or nodal nature of the superconducting gap. The well-fitted data using the isotropic s-wave model has revealed a moderately coupled nature of samples. ZF-μSR data reveals a difference in the asymmetry spectra as temperature goes below T_c. However, fitting parameters show a gradual increase, ruling out the presence of any spontaneous field below T_c, which can otherwise give a sudden increase in relaxation rate at T_c. This behavior can be attributed to electronic fluctuations measurable within the μSR timescale. It is also noteworthy that LaNiSi with low ASOC has shown a stronger electronic fluctuation. A recent report on noncentrosymmetric $Re_{5.5}Ta$ by Arushi *et al.* has shown spin fluctuation behavior [61], while similar other Re-based compounds from the family have shown TRSB. These evidences call for more investigations to elucidate the correlation between ASOC, spin fluctuation, and the presence/absence of time-reversal symmetry.

ACKNOWLEDGMENTS

R.P.S. acknowledges Science and Engineering Research Board, Government of India for the Core Research Grant No. CRG/2019/0010282. We thank Newton Bhabha for funding and ISIS, STFC, UK, for the muon beam time to conduct the μSR experiments.

[1] E. Bauer and M. Sigrist, *Non-Centrosymmetric Superconductor: Introduction and Overview* (Springer-Verlag, Heidelberg, 2012).
[2] M. Smidman, M. B. Salamon, H. Q. Yuan, and D. F. Agterberg, Rep. Prog. Phys. **80**, 036501 (2017).
[3] A. P. Schnyder and S. Ryu, Phys. Rev. B **84**, 060504(R) (2011).
[4] L. P. Gor'kov and E. I. Rashba, Phys. Rev. Lett. **87**, 037004 (2001).
[5] P. A. Frigeri, D. F. Agterberg, and M. Sigrist, New J. Phys. **6**, 115 (2004).
[6] V. M. Edel'shtein, Sov. Phys. JETP **68**, 1244 (1989).
[7] S. Fujimoto, J. Phys. Soc. Jpn. **76**, 051008 (2007).
[8] K. V. Samokhin, E. S. Zijlstra, and S. K. Bose, Phys. Rev. B **69**, 094514 (2004).
[9] P. A. Frigeri, D. F. Agterberg, A. Koga, and M. Sigrist, Phys. Rev. Lett. **92**, 097001 (2004).
[10] E. Bauer, G. Hilscher, H. Michor, Ch. Paul, E. W. Scheidt, A. Gribanov, Y. Seropegin, H. Noël, M. Sigrist, and P. Rogl, Phys. Rev. Lett. **92**, 027003 (2004).
[11] I. Bonalde, W. Brämer-Escamilla, and E. Bauer, Phys. Rev. Lett. **94**, 207002 (2005).
[12] M. Nishiyama, Y. Inada, and G.-Q. Zheng, Phys. Rev. Lett. **98**, 047002 (2007).
[13] Y. Tanaka, Y. Mizuno, T. Yokoyama, K. Yada, and M. Sato, Phys. Rev. Lett. **105**, 097002 (2010).
[14] X. L. Qi and S. C. Zhang, Rev. Mod. Phys. **83**, 1057 (2011).
[15] H. Q. Yuan, D. F. Agterberg, N. Hayashi, P. Badica, D. Vandervelde, K. Togano, M. Sigrist, and M. B. Salamon, Phys. Rev. Lett. **97**, 017006 (2006).
[16] S. Harada, J. J. Zhou, Y. G. Yao, Y. Inada, and G.-Q. Zheng, Phys. Rev. B **86**, 220502(R) (2012).
[17] H. Mukuda, T. Fujii, T. Ohara, A. Harada, M. Yashima, Y. Kitaoka, Y. Okuda, R. Settai, and Y. Onuki, Phys. Rev. Lett. **100**, 107003 (2008).
[18] G. M. Pang, M. Smidman, W. B. Jiang, J. K. Bao, Z. F. Weng, Y. F. Wang, L. Jiao, J. L. Zhang, G. H. Cao, and H. Q. Yuan, Phys. Rev. B **91**, 220502(R) (2015).
[19] D. T. Adroja, A. Bhattacharyya, M. Telling, Yu. Feng, M. Smidman, B. Pan, J. Zhao, A. D. Hillier, F. L. Pratt, and A. M. Strydom, Phys. Rev. B **92**, 134505 (2015).
[20] J. Chen, L. Jiao, J. L. Zhang, Y. Chen, L. Yang, M. Nicklas, F. Steglich, and H. Q. Yuan, New J. Phys. **15**, 053005 (2013).
[21] S. Kuroiwa, Y. Saura, J. Akimitsu, M. Hiraishi, M. Miyazaki, K. H. Satoh, S. Takeshita, and R. Kadono, Phys. Rev. Lett. **100**, 097002 (2008).
[22] M. Z. Hasan and C. L. Kane, Rev. Mod. Phys. **82**, 3045 (2010).
[23] A. P. Schnyder, P. M. R. Brydon, and C. Timm, Phys. Rev. B **85**, 024522 (2012).
[24] A. P. Schnyder and P. M. R. Brydon, J. Phys.: Condens. Matter. **27**, 243201 (2015).
[25] M. Z. Hasan and J. E. Moore, Ann. Rev. Condens. Matter Phys. **2**, 55 (2011).
[26] C. Q. Xu, B. Li, J. J. Feng, W. H. Jiao, Y. K. Li, S. W. Liu, Y. X. Zhou, R. Sankar, N. D. Zhigadlo, H. B. Wang, Z. D. Han, B. Qian, W. Ye, W. Zhou, T. Shiroka, P. K. Biswas, X. Xu, and Z. X. Shi, Phys. Rev. B **100**, 134503 (2019).
[27] J. A. T. Barker, D. Singh, A. Thamizhavel, A. D. Hillier, M. R. Lees, G. Balakrishnan, D. McK. Paul, and R. P. Singh, Phys. Rev. Lett. **115**, 267001 (2015).
[28] R. P. Singh, A. D. Hillier, B. Mazidian, J. Quintanilla, J. F. Annett, D. M. Paul, G. Balakrishnan, and M. R. Lees, Phys. Rev. Lett. **112**, 107002 (2014).
[29] D. Singh, J. A. T. Barker, A. Thamizhavel, D. McK. Paul, A. D. Hillier, and R. P. Singh, Phys. Rev. B **96**, 180501(R) (2017).
[30] D. Singh, Sajilesh K. P., J. A. T. Barker, D. M. Paul, A. D. Hillier, and R. P. Singh, Phys. Rev. B **97**, 100505(R) (2018).
[31] A. D. Hillier, J. Quintanilla, and R. Cywinski, Phys. Rev. Lett. **102**, 117007 (2009).

[32] J. Quintanilla, A. D. Hillier, J. F. Annett, and R. Cywinski, Phys. Rev. B **82**, 174511 (2010).

[33] A. D. Hillier, J. Quintanilla, B. Mazidian, J. F. Annett, and R. Cywinski, Phys. Rev. Lett. **109**, 097001 (2012).

[34] P. K. Biswas, M. R. Lees, A. D. Hillier, R. I. Smith, W. G. Marshall, and D. M. Paul, Phys. Rev. B **84**, 184529 (2011).

[35] A. B. Karki, Y. M. Xiong, I. Vekhter, D. Browne, P. W. Adams, D. P. Young, K. R. Thomas, J. Y. Chan, H. Kim, and R. Prozorov, Phys. Rev. B **82**, 064512 (2010).

[36] R. P. Singh, A. D. Hillier, D. Chowdhury, J. A. T. Barker, D. M. Paul, M. R. Lees, and G. Balakrishnan, Phys. Rev. B **90**, 104504 (2014).

[37] E. Bauer, R. T. Khan, H. Michor, E. Royanian, A. Grytsiv, N. Melnychenko-Koblyuk, P. Rogl, D. Reith, R. Podloucky, E.-W. Scheidt, W. Wolf, and M. Marsman, Phys. Rev. B **80**, 064504 (2009).

[38] Sajilesh K. P., D. Singh, P. K. Biswas, A. D. Hillier, and R. P. Singh, Phys. Rev. B **98**, 214505 (2018).

[39] T. Shang, M. Smidman, S. K. Ghosh, C. Baines, L. J. Chang, D. J. Gawryluk, J. A. T. Barker, R. P. Singh, D. McK. Paul, G. Balakrishnan, E. Pomjakushina, M. Shi, M. Medarde, A. D. Hillier, H. Q. Yuan, J. Quintanilla, J. Mesot, and T. Shiroka, Phys. Rev. Lett. **121**, 257002 (2018).

[40] K. Klepp and E. Parthe, Acta Cryst. B **38**, 1105 (1982).

[41] W. H. Lee, F. A. Yang, and C. R. Shih, and H. D. Yang, Phys. Rev. B **50**, 6523(R) (1994).

[42] S. Ramakrishnan, K. Ghosh, A. D. Chinchure, V. R. Marathe, and G. Chandra, Phys. Rev. B **52**, 6784 (1995).

[43] A. Ptok, K. Domieracki, K. J. Kapcia, J. Lazewski, P. T. Jochym, M. Sternik, P. Piekarz, and D. Kaczorowski, Phys. Rev. B **100**, 165130 (2019)

[44] P. Zhang, H. Yuan, and C. Cao, Phys. Rev. B **101**, 245145 (2020)

[45] F. Kneidinger, H. Michor, A. Sidorenko, E. Bauer, I. Zeiringer, P. Rogl, C. Blaas-Schenner, D. Reith, and R. Podloucky, Phys. Rev. B **88**, 104508 (2013).

[46] G. M. Luke, A. Keren, L. P. Le, W. D. Wu, Y. J. Uemura, D. A. Bonn, L. Taillefer, and J. D. Garrett, Phys. Rev. Lett. **71**, 1466 (1993).

[47] Y. Aoki, A. Tsuchiya, T. Kanayama, S. R. Saha, H. Sugawara, H. Sato, W. Higemoto, A. Koda, K. Ohishi, K. Nishiyama, and R. Kadono, Phys. Rev. Lett. **91**, 067003 (2003).

[48] R. Khasanov, K. Conder, E. Pomjakushina, A. Amato, C. Baines, Z. Bukowski, J. Karpinski, S. Katrych, H. H. Klauss, H. Luetkens, A. Shengelaya, and N. D. Zhigadlo, Phys. Rev. B **78**, 220510(R) (2008).

[49] S. L. Lee, S. H. Kilcoyne, and R. Cywinski, *Muon Science: Muons in Physics, Chemistry and Materials* (SUSSP Publications and IOP Publishing, Bristol, 1999).

[50] R. S. Hayano, Y. J. Uemura, J. Imazato, N. Nishida, T. Yamazaki, and R. Kubo, Phys. Rev. B **20**, 850 (1979).

[51] J. A. T. Barker, R. P. Singh, A. D. Hillier, and D. McK. Paul, Phys. Rev. B **97**, 094506 (2018).

[52] T. Shang, A. Amon, D. Kasinathan, W. Xie, M. Bobnar, Y. Chen, A. Wang, M. Shi, M. Medarde, H. Q. Yuan, and T. Shiroka, New J. Phys. **21**, 073034 (2019).

[53] A. Bhattacharyya, P. P. Ferreira, F. B. Santos, D. T. Adroja, J. S. Lord, L. E. Correa, A. J. S. Machado, A. L. R. Manesco, and L. T. F. Eleno, Phys. Rev. Res. **2**, 022001 (2020).

[54] E. H. Brandt, J. Low Temp. Phys. **73**, 355 (1988).

[55] E. H. Brandt, Phys. Rev. B **68**, 054506 (2003).

[56] D. Singh, Sajilesh K. P., S. Marik, A. D. Hillier, and R. P. Singh, Phys. Rev. B **99**, 014516 (2019).

[57] Y. J. Uemura, V. J. Emery, A. R. Moodenbaugh, M. Suenaga, D. C. Johnston, A. J. Jacobson, J. T. Lewandowski, J. H. Brewer, R. F. Kiefl, S. R. Kreitzman, G. M. Luke, T. Riseman, C. E. Stronach, W. J. Kossler, J. R. Kempton, X. H. Yu, D. Opie, and H. E. Schone, Phys. Rev. B **38**, 909(R) (1988).

[58] Y. J. Uemura, G. M. Luke, B. J. Sternlieb, J. H. Brewer, J. F. Carolan, W. N. Hardy, R. Kadono, J. R. Kempton, R. F. Kiefl, S. R. Kreitzman, P. Mulhern, T. M. Riseman, D. L. Williams, B. X. Yang, S. Uchida, H. Takagi, J. Gopalakrishnan, A. W. Sleight, M. A. Subramanian, C. L. Chien, M. Z. Cieplak, G. Xiao, V. Y. Lee, B. W. Statt, C. E. Stronach, W. J. Kossler, and X. H. Yu, Phys. Rev. Lett. **62**, 2317 (1989).

[59] Y. J. Uemura, L. P. Le, G. M. Luke, B. J. Sternlieb, W. D. Wu, J. H. Brewer, T. M. Riseman, C. L. Seaman, M. B. Maple, M. Ishikawa, D. G. Hinks, J. D. Jorgensen, G. Saito, and H. Yamochi, Phys. Rev. Lett. **66**, 2665 (1991).

[60] A. D. Hillier and R. Cywinski, Appl. Magn. Reson. **13**, 95 (1997).

[61] Arushi, D. Singh, P. K. Biswas, A. D. Hillier, and R. P. Singh, Phys. Rev. B **101**, 144508 (2020).